



# Comparison of state-of-the-art machine learning algorithms and data-driven optimization methods for mitigating nitrogen crossover in PEM fuel cells



Jiankang Wang<sup>a</sup>, Rui Ding<sup>a</sup>, Feng Cao<sup>a</sup>, Jia Li<sup>a</sup>, Hui Dong<sup>d</sup>, Tao Shi<sup>e</sup>, Lei Xing<sup>c,\*</sup>,  
Jianguo Liu<sup>a,b,\*</sup>

<sup>a</sup> National Laboratory of Solid State Microstructures, College of Engineering and Applied Sciences, Nanjing University, 22 Hankou Road, Nanjing 210093, PR China

<sup>b</sup> Institute of Energy Power Innovation, North China Electric Power University, 2 Beinong Road, Beijing 102206, PR China

<sup>c</sup> Department of Engineering Science, University of Oxford, Oxford OX1 3PJ, United Kingdom

<sup>d</sup> Pearl Hydrogen Technology Co., Ltd., No. 1979, Chengqiao Rd, Fengxian District, Shanghai, PR China

<sup>e</sup> Pearl Hydrogen (Foshan) Technology Co., Ltd., 6th Floor, Complex Building A1, No.10 Guanjin Rd., Danzao, Nanhui District, Foshan, Guangdong, PR China

## ARTICLE INFO

### Keywords:

PEM fuel cell

N<sub>2</sub> crossover

Multi-variable optimization

AI

Machine learning

## ABSTRACT

Nitrogen gas crossover (NGC) and nitrogen accumulation at the anode of proton exchange membrane (PEM) fuel cells are ineluctable and it would lead to inferior performance and even irreversible damage to functional components. To mitigate this issue, multiphysics numerical models (MNMs) are established to describe NGC behaviors and further guide experimental studies. However, to obtain the optimized parameters that would suppress NGC and retain high performance, grid search conducted on MSMs would cost unaffordable computational resources and time. Therefore, we innovatively introduced a machine learning-assisted MNM (MSM-ML) as a surrogate model, in which 9 state-of-the-art machine learning algorithms were compared, to greatly boost the resolution of this engineering problem. Through the proposed MSM-ML workflow performed on an experimentally validated MSM, the cost for obtaining the best parameter combination is greatly reduced. Moreover, the impact of each parameter in this complex system is directly revealed through the application of black-box interpretation methods afterwards. As a result, a new approach was pioneered to solve engineering problems which was demonstrated to be more efficient and intelligent than traditional methods. The NGC coefficient is reduced by 49.5%, while the power density is improved by 20% through the multivariable optimization of the developed MSM-ML.

## 1. Introduction

As an important part of a future renewable energy-driven society, the utilization of hydrogen energy requires proton exchange membrane (PEM) fuel cells as energy conversion devices. Economics and stability are the two major issues that must be overcome in the process of large-scale commercialization of PEM fuel cells. Despite the progress made, there are some technical difficulties for which no great solution has yet

been found. One of them is the nitrogen gas crossover (NGC) phenomenon and accompanied nitrogen accumulation at the anode of PEM fuel cells [1]. Gas crossover refers to the phenomenon that the feed gas inevitably penetrates the ion cluster and the amorphous part of the hydrophobic backbone of the membrane under the pressure gradient during the operation of fuel cells and reaches the anode side of PEM fuel cells. To reduce the tail of hydrogen and improve utilization efficiency during the operation of high-power PEM fuel cells, anode effluent gas is

**Abbreviations:** NGC, Nitrogen gas crossover; PEM, Proton exchange membrane; MNMs, Multiphysics numerical models; MSM-ML, Machine learning-assisted MNM; AI, Artificial intelligence; ACH, Anode flow channel; CCH, Cathode flow channel; AGDL, Anode gas diffusion layer; CGDL, Cathode gas diffusion layer; ACL, Anode catalytic layer; CCL, Cathode catalytic layer; SI, Supporting information; XGBoost, Extreme gradient boosting; Gradientboost, Gradient boosting; CatBoost, Categorical boosting; LightGBM, Light gradient boosting machine; AdaBoost, Adaptive Boosting; ANN, Artificial neural network; SHAP, Shapley additive explanations.

\* Corresponding authors at: National Laboratory of Solid State Microstructures, College of Engineering and Applied Sciences, Nanjing University, 22 Hankou Road, Nanjing 210093, China.

E-mail addresses: [lei.xing@eng.ox.ac.uk](mailto:lei.xing@eng.ox.ac.uk), [xinglei1314@gmail.com](mailto:xinglei1314@gmail.com) (L. Xing), [jianguoliu@nju.edu.cn](mailto:jianguoliu@nju.edu.cn) (J. Liu).

<https://doi.org/10.1016/j.cej.2022.136064>

Received 16 December 2021; Received in revised form 8 March 2022; Accepted 25 March 2022

Available online 28 March 2022

1385-8947/© 2022 Elsevier B.V. All rights reserved.

usually recycled in current PEM fuel cells. However, nitrogen inevitably accumulates at the anode electrode due to the hydrogen recirculation systems after long-term operation, which causes local fuel starvation at the anode and then leads to carbon corrosion [2–5], resulting in an irreversible decline in the cell performance. High-frequency periodic purging of the accumulated nitrogen also causes a large amount of fuel waste and lower cell performance in the purge process [6,7]. Therefore, it is of great significance to reduce NGC by optimizing the operating conditions and geometric structure of PEM fuel cells.

Obviously, NGC, as a diffusion control process, is greatly affected by the structure and operating conditions. Determinant parameters are membrane thickness[8], diffusion layer thickness[8], operating temperature[9], operating pressure[10], relative humidity of reactant gases [8,11]. Previous experimental results have shown that the increase in temperature, pressure and relative humidity reinforces the NGC coefficient and the influence of membrane thickness is more complex [9,12–14]. The relative humidity and temperature effects are more significant since the SO<sub>3</sub> functional groups at the end of the Nafion molecule are strongly hydrophilic [15]. The new Nafion 211 membrane, which is cast from dispersion and has different water absorption properties compared with traditional Nafion membranes, shows different gas crossover rates, which verifies the micellar network mechanism [16]. The main reason for the effect of temperature on gas crossover is that the thermal expansion coefficient of the amorphous phase is larger than that of the crystalline phase. Although it is of great significance to investigate the impact of different parameters independently, a comprehensive consideration that takes both NGC and cell performance into concern would make the multi-target optimization in such parametric space an extremely complicated process. As the cost of the experiment is unacceptable, it is necessary to seek simulation tools for assistance.

With the development of computer technology, a large number of multiphysics numerical models (MNM)s have been developed to study the influence of operating conditions and geometric structure by establishing steady-state PEM fuel cell models. Li et al. [17] built a three-dimensional, multiphase numerical model to analyze the optimal slope angle of the wave structure of a PEM fuel cell. Nguyen et al. [8,18] numerically investigated the effects of gas crossover across membranes under different operating conditions and geometric parameters in a PEM fuel cell. These studies only focus on few parameters. Only the vague impact of each parameter was simulated in these studies, and a clear combination of the studied parameters that might lead to optimum cell performance was not provided due to the complexity of the model. Meanwhile, conducting a grid-search on an MNM for potential optimal values requires considerable computational resources and time. If it is necessary to improve the density of the grid search or improve the optimization search dimensions, the calculation cost will increase exponentially. Therefore, although the MNM could accurately describe the behaviors of PEM fuel cells, along with the detailed electrochemical and transport processes involved, the utilization of MNM for direct guidance is often limited due to the extremely heavy computation load and long calculation time.

Machine learning is a common research hotspot in the field of artificial intelligence (AI) and pattern recognition and has proven to be effective in boosting the field of natural science and engineering research, especially for complex systems such as PEM fuel cells. Ding et al.[19,20] firstly introduced machine learning (ML) to determine the key parameters for nonprecious metal electrocatalyst-based PEM fuel cells. Hua et al.[21] studied the effectiveness of machine learning algorithms on predicting the remaining useful life of PEM fuel cell. Xing et al.[22] used the Kriging (KRG) surrogate model to evaluate the optimal values of five design variables of the catalyst layer with respect to two objective functions. Machine learning models are data-driven and require relatively small computational resources while maintaining high accuracy in predicting the behaviors of PEM fuel cells. This trait could help researchers easily overcome the previously unaffordable time cost for multivariable optimization. As previously mentioned, designing PEM

fuel cells would greatly benefit if the MNM could be replaced by machine learning surrogate models.

Herein, we propose an MNM-ML approach to accelerate the optimization of engineering problems in PEM fuel cells, taking NGC optimization as an example, as illustrated in Fig. 1. First, we built a highly accurate MNM of PEM fuel cells describing N<sub>2</sub> crossover, which is well verified by experiments. To reduce the high computational cost, a database was built by varying operating conditions and geometric structures at appropriate intervals. Different algorithms were trained on the developed machine learning surrogate models, and a hyper-parameter grid search was conducted to obtain the best model with the highest reproducibility of the original MNM. For better comprehension of the impact brought by each parameter, interpretation methods SHapley Additive exPlanations (SHAP) were applied to directly illustrate the patterns in the complex system. Finally, genetic algorithm was used to obtain the optimal parameter combination containing operating conditions and geometric structures. Compared with the values without optimization, the nitrogen crossover coefficient was successfully reduced by 49.5% in 6 important dimensions, with the performance improved by 20%. More significantly, the computation time for searching for such an optimal value has been reduced from several months to a few days. This strategy, as proposed in this work, could not only be used to mitigate NGC but also be extended to other complex optimization tasks at the system level.

## 2. MNM-ML

A machine learning-assisted multiphysics numerical model (MNM-ML) based on a new engineering optimization approach, as shown in Fig. 1, is proposed, which mainly includes four parts: establishment and validation of MNM, database construction, machine learning surrogate modeling and, finally, multivariable optimization.

### 2.1. Establishment and validation of MNM

A two-dimensional steady-state model is accomplished on the commercial software platform COMSOL Multiphysics 5.5a to describe the NGC in a PEM fuel cell, as shown in Fig. 2, which includes seven key components: anode flow channel (ACH), cathode flow channel (CCH), anode gas diffusion layer (AGDL), cathode gas diffusion layer (CGDL), anode catalytic layer (ACL), cathode catalytic layer (CCL) and PEM. The model consists of conservation equations of mass, species, momentum, charge and energy, and the governing equations of gas crossover and water management are mutually added and coupled with each other. The details of the governing equations are shown in Eq. (1) to Eq. (55) in Supporting Information (SI), which are mainly based on the multiphysics and two-phase flow model developed previously[8,22–32]. Then, free triangular meshing was built on the geometric model. The maximum element was set as  $3.0 \times 10^{-4}$  to guarantee the precision of the numerical solution of the model. The boundary layer was set at the junction of the PEM, ACL, CCL and other fine components to improve the astringency of the model. In the computational process, all physical quantities were given reasonable initial values at the nodes of the grid, and then the iterative solution was carried out under the constraints of the governing equation until the error was less than  $1.0 \times 10^{-4}$ . Finally, the numerical solution of the two-dimensional steady state model was obtained. In addition, the details of experimental validation of the developed PEM fuel cell model and the further experimental studies regarding the influence of N<sub>2</sub> crossover are shown in SI.

### 2.2. Database construction

Based on previous reports [7,12,33,34], six major parameters that greatly affect NGC are selected: the PEM thickness ( $\delta_M$ ), GDL thickness ( $\delta_{GDL}$ ), flow channel depth ( $\delta_{CH}$ ), operating temperature at current collector ( $T_{cc}$ ), operating pressure ( $P_A$ ) and relative humidity of reactant

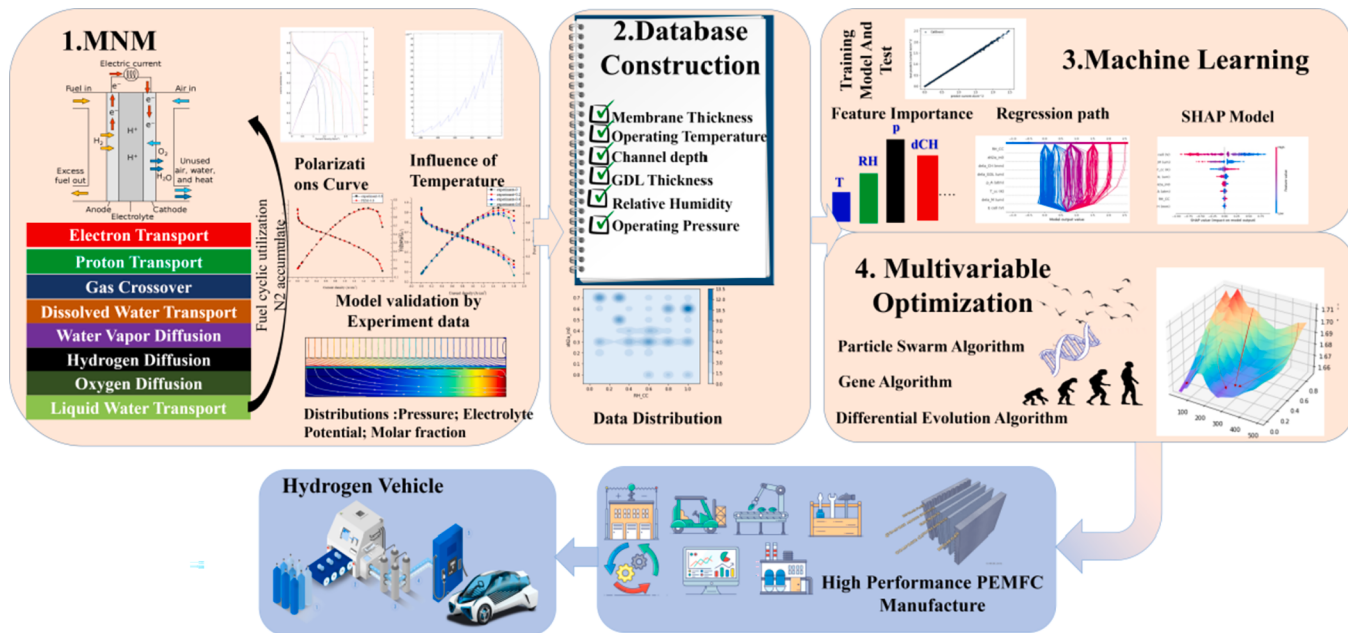
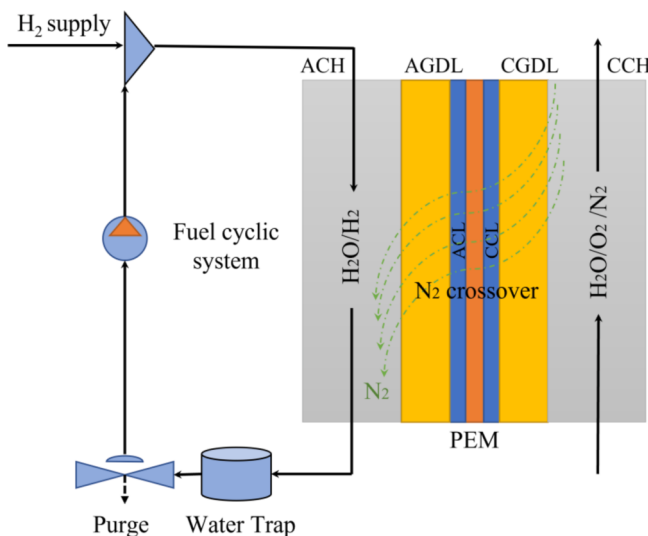


Fig. 1. MNM-ML workflow.

Fig. 2. Sketch of a polymer electrolyte membrane fuel cell and the  $N_2$  crossover phenomenon.

gas in current collector ( $RH_{cc}$ ). A grid strategy formed by combination of sparse grid sampling methods and random sampling technique, as shown in **Figure S1**, is adapted to establish the database, which is considered as a more convenient and efficient process to gradually enrich the database until desirable accuracy of the trained model is achieved. It took 3 days (details of the workstation are shown in the section 8 of the SI). The polarization curves and NGC coefficients are obtained by solving the MNMs in grided parameter space, and a six-dimensional database consisting of 3000 sets is established. The original database is available as an additional file from the accompanying GitHub link.

### 2.3. Machine learning surrogate modeling

The third step is to use the database to train 9 state-of-the-art and explainable (selection criteria) algorithms widely used in the field of machine learning, including extreme gradient boosting (XGBoost) [35],

gradient boosting (Gradientboost) [36], categorical boosting (CatBoost) [37], random forest [38], extra tree [39], decision tree [40], light gradient boosting machine (LightGBM) [41], adaptive boosting (AdaBoost) [42] and artificial neural network (ANN) [43]. Brief introduce of the nine algorithms are available in the SI. To obtain the best surrogate models, combinations of hyperparameters are optimized through adaptive grid optimization. Fivefold cross-validation was performed to evaluate the regression performance. As a result, the best machine learning surrogate model was obtained that would give almost the same results, but the computational cost is tens of thousands of times less than that of the original MNM. The use of this surrogate model greatly shortens the time and computational cost of the multivariable optimization of engineering problems. For model interpretation, the SHAP package [44,45] was used to explain the impact and importance degree of each parameter in the surrogate model.

### 2.4. Multivariable optimization

The fourth step is to conduct global adaptive search iteration on the machine learning surrogate model through advanced optimization algorithms such as the genetic algorithm (GA), particle swarm optimization algorithm (PSO) and differential evolution (DE) to find the optimal combination of the 6 parameters and corresponding output value of the nitrogen crossover coefficient and current density.

### 2.5. GitHub link

<https://github.com/wjkangjian/N2-gas-crossover->

## 3. Results and discussion

### 3.1. Validation of multiphysics numerical model

As the first step of the workflow, the reliability of the MNM should be validated. The polarization curves under different degrees of nitrogen accumulation obtained by experiments and the MNM are shown in **Fig. 3a-e**. The experiment validation details are shown in the first section of SI. Clearly, the experimental results are highly consistent with the solution of the MNM. The average deviation of the current density is only  $0.05 \text{ A cm}^{-2}$  at  $0.6 \text{ V}$ , which proves the reliability of the developed

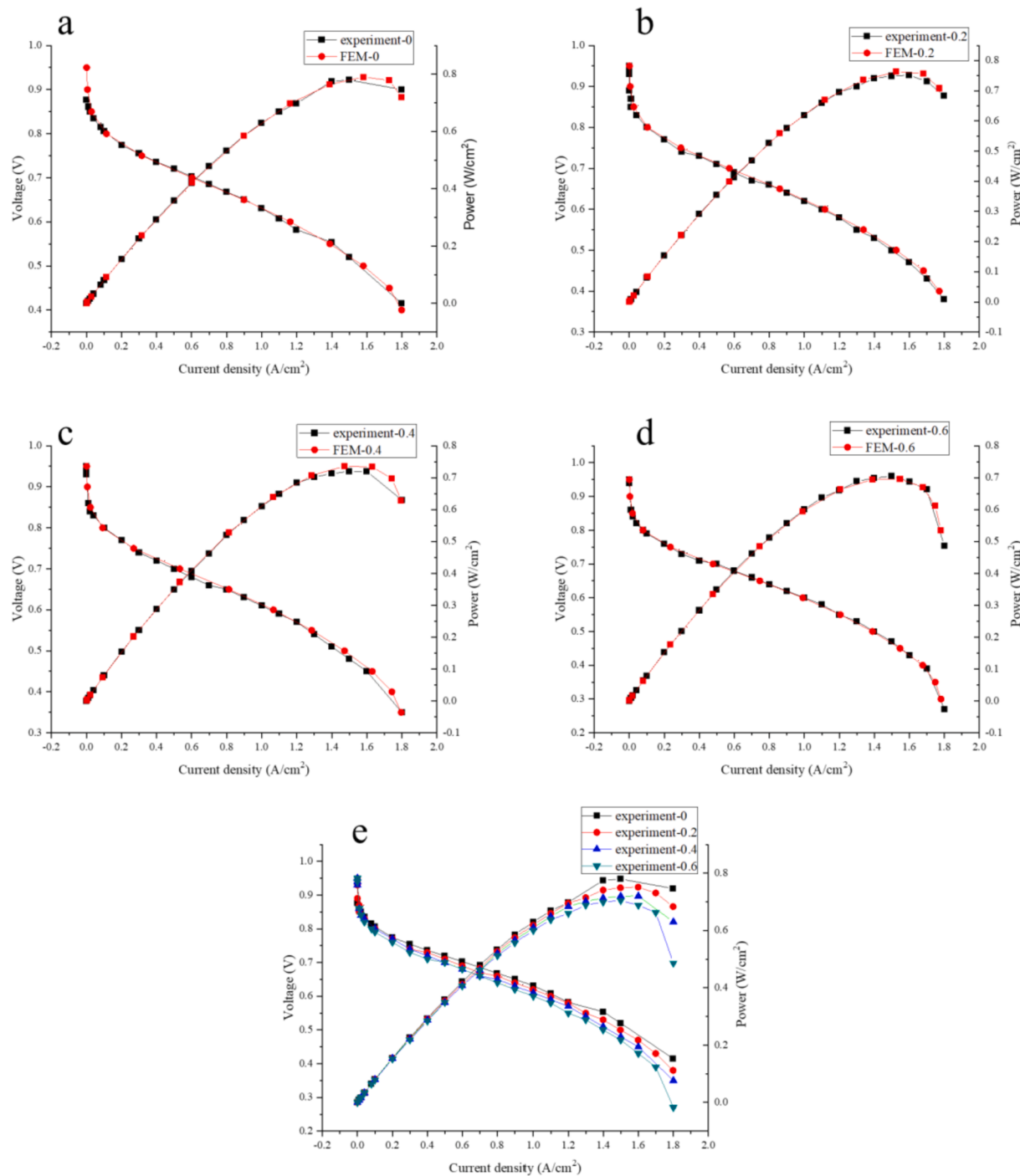


**Fig. 3.** Polarization curves of the MNM model and experimental validation when the volume fraction of  $N_2$  was a). 0b). 0.2c). 0.4 d). 0.6. e). Comparison of the cell performance under different NGCs.

MNM.

The comparison of polarization curves of the cell under different degrees of nitrogen accumulation is shown in Fig. 3e. It is obvious that anode nitrogen accumulation reduces the overall performance of the cell. NGC leads to a decrease in hydrogen concentration in the polarized activation region and thereby a slower reaction rate and worse cell performance. When the current density increases, this effect becomes more severe in the mass transfer control zone. When the cumulative nitrogen mole fraction reached 0.6, the decrease in the maximum power density occurred at  $1.5 \text{ A cm}^{-2}$ , reaches up to 10.1%. The maximum cell power density loss is found to be 28.9% at a current density of  $1.8 \text{ A cm}^{-2}$ .

Despite that MNM could well describe the detailed behavior of PEM fuel cells, using it to obtain optimal design parameters for experimental or manufacturing guidance is not feasible because it takes approximately  $2 \sim 5$  mins to compute a single model. Thus, solving the parameters gridded model of 6 dimensions with 5 values would cost  $5^6 = 15625$  min, which is 22 days. A finer grid-search process would cost more time that might be hardly affordable. Therefore, it is of great significance to introduce the machine learning surrogate model to avoid unacceptable time costs.

### 3.2. Machine learning surrogate model training

After the database was established as described in section 2.2, the database was divided into a training set (85%) and a test set (15%). The training set data were used to train the machine learning models. The best hyperparameters of the machine learning algorithms of N<sub>2</sub> crossover regression and current density regression are shown in Table S2 and Table S3 in the SI, respectively. The test set data was used to evaluate the models. Taking the best performing ANN and XGBoost as examples, the predictions made by machine learning models and the original MNM are illustrated in Fig. 4. For each point in the scatter diagram, the x-coordinate is the predicted values by the machine learning model, and the y-coordinate is the actual values obtained from the MNM in the test set database. Thus, the closer a point is to the light blue slash “y = x”, the closer the predicted value is to the true value. Then, the validity of the model can be expressed by the correlation coefficient ( $R^2$ ) of the scatter to the “y = x” oblique line. Figure S2 and S3 in the SI show the model effectiveness of the other 8 machine learning algorithms for current density prediction and NGC coefficient prediction, respectively. It is easy to conclude that all the machine learning algorithms used are very accurate and efficient for data database learning because the  $R^2$  values are almost all over 0.97. Therefore, root mean square error (RMSE) is introduced to further evaluate the accuracy of the model.

As shown in Fig. 5, for current density prediction, the ANN algorithm has the smallest root mean square error, which is only 0.006, while the AdaBoost algorithm has the largest root mean square error of 0.13, which is 21 times that of the former algorithm. This also further indicates that there is no algorithm, and it is necessary to select the optimal algorithm through the competition of various algorithms. In

general, XGBoost is the most suitable algorithm for predicting the gas crossover, reflected by the computed NGC coefficient. These two models could replace the original MNM model for quick parametric optimization.

### 3.3. Machine learning surrogate model explanation

Although the machine learning surrogate models have been obtained with excellent performance, the black-box nature of the model determines the reduction credibility of the model and blocks the possibility of further research on scientific problems. We used the open-source package SHAP to study and explain the internal process of the machine learning algorithms, that was used to improve the reliability of the model. As a result, the predictive interpretation of the model is highly consistent with the literature and prior knowledge.

The internal regression paths of the machine learning model of six algorithms that perform well on the fuel cell gas crossover task, including XGBoost, LightGBM, Extra Tree, Decision Tree, CatBoost and Gradient Boost, are shown in Fig. 6. The upper x-coordinate is the model output values, and the colorful gradient is determined to express the output values and keep the regression paths clearer. The lower x-coordinate is the base value that is always defined as the global mean. The y-coordinate is the model input parameters. The routes from the lower x-coordinate to the upper x-coordinate are determined by the parameters we concerned, which are listed in the y-coordinate. As annotated in Fig. 6d, each step is corresponding to each parameter, the length of which along the x direction means the importance of the parameters on single sample. Although the basic frameworks of the adopted algorithms are completely different, highly similar regression paths are obtained for

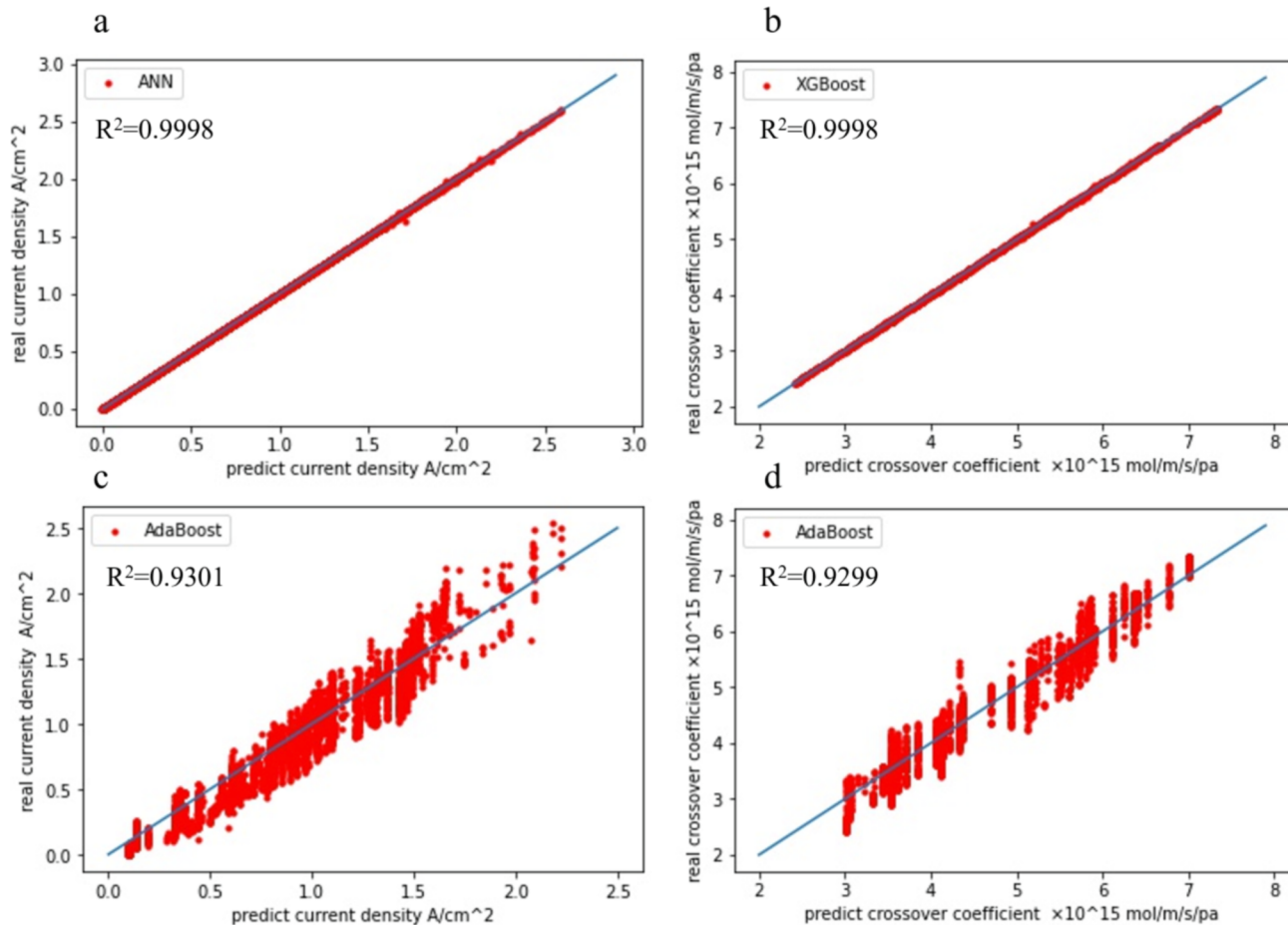


**Fig. 4.** a). Predictions of the ANN test set for current density regression, b). Predictions of the XGBoost test set for N<sub>2</sub> crossover regression, c). Prediction of the AdaBoost test set for current density regression, d). Predictions of the AdaBoost test set for N<sub>2</sub> crossover regression.

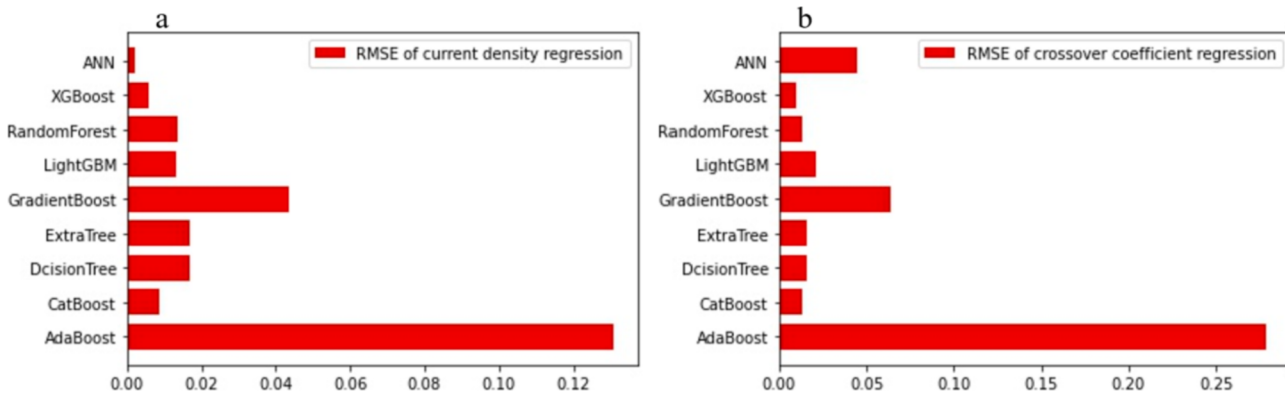


Fig. 5. RMSE of each algorithm for a). current density regression, b). N<sub>2</sub> crossover regression.

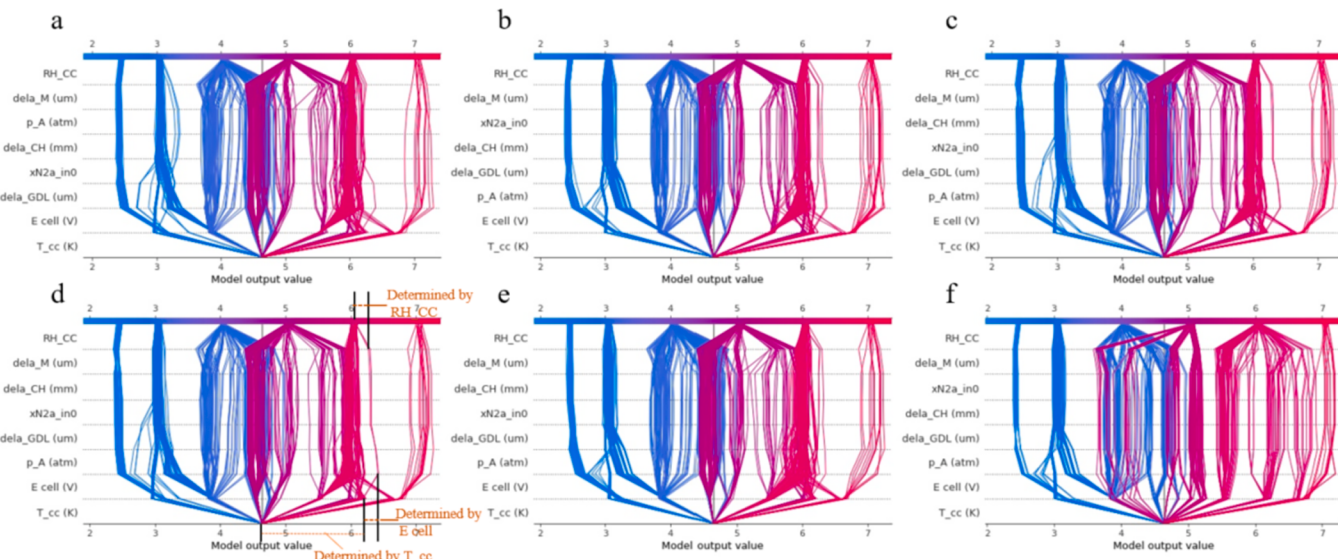


Fig. 6. regression path of a). XGBoost, b). LightGBM, c). ExtraTree, d). DecisionTree, e). CatBoost, f). GradientBoost for crossover coefficient. (The unit of the model output value is  $\times 10^{-15}$  mol m<sup>-1</sup> s<sup>-1</sup> Pa<sup>-1</sup>).

the samples in the database. The high degree of consistency reflects the accuracy of the machine learning algorithm. It is worth mentioning that the poorly performing gradient boost algorithm is significantly different from the other five algorithms in the crossover region, which could explain its large root mean square error. It is mainly derived from the regression of the high gas crossover region (red curves). The prediction path of machine learning algorithms for current density regression is

shown in Figure S4 in the SI, and a similar phenomenon occurs.

#### 3.4. Parameter importance

As commonly adopted as a perfect explanation method to reveal the qualitative and quantitative impact of input parameters on the output target, SHAP values are the quantification of the influence degree of

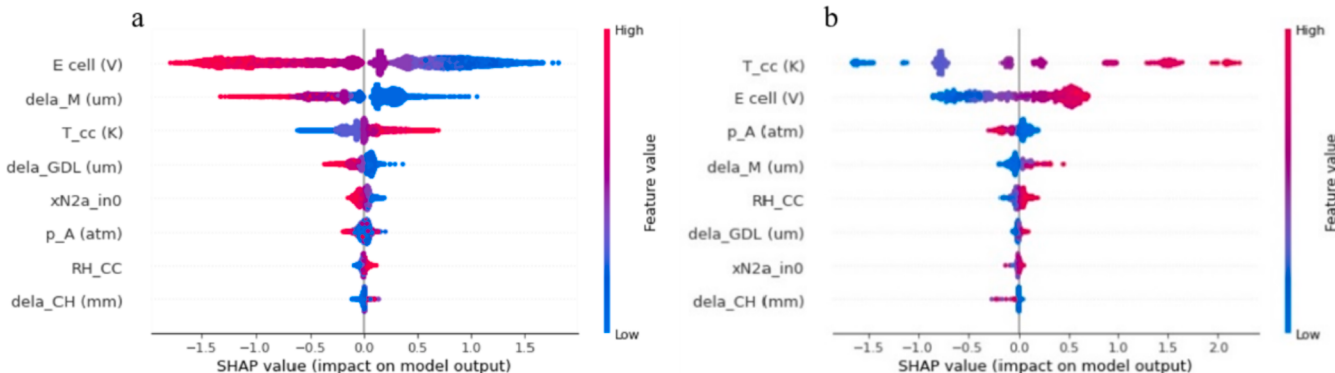


Fig. 7. SHAP values summary plots of, a). the ANN model for current density regression and b). the XGBoost model for N<sub>2</sub> crossover regression (width in y direction results from the degree of the aggregation of the sample points).

different parameters on the predicted value. When it is greater than 0, it indicates that the current value of the corresponding input parameter improves the output value; otherwise, it reduces the output value. Larger absolute values of SHAP represent a greater impact of the corresponding parameters. A brief introduction of this method is available in the SI.

The SAHP value distributions of all parameters of the ANN model for current density prediction and the XGBoost model for N<sub>2</sub> crossover prediction are shown in Fig. 7. The SAHP value distributions of the other algorithms are shown in Figure S5 and S6 in the SI. The x-coordinate is the SHAP value (impact on model output), and the y-coordinates are the 6 studied input parameters. The color represents the parameter value of each sample. The warmer the colors represent higher feature values. The width along the y direction influences the shape of the SHAP values, which is determined by the degree of the aggregation of sample points in the same SHAP value (x coordinate values) and the dispersion degree in  $\times$  direction, that is further influenced by the sampling interval and the importance of each parameter for the model output. Higher parameter importance results in higher dispersion degree in  $\times$  direction. In reverse, higher dispersion degree shows higher parameter importance. We can easily see from the ANN regression model that the most important factor affecting the current density is the cell voltage. The operating temperature is the most significant factor for N<sub>2</sub> crossover in the XGBoost model. Having compared all different models, we can easily conclude that the parameter importance ranking for current density is cell voltage, followed by membrane thickness, operating temperature, GDL thickness, the degree of N<sub>2</sub> accumulation, relative humidity and channel depth in descending order. The cell voltage, membrane thickness, GDL thickness, and N<sub>2</sub> accumulation degree negatively correlate with current density, and the others are positively related. Similarly, we could conclude that the parameter importance ranking for N<sub>2</sub> crossover is operating temperature, followed by the cell voltage, operating pressure, membrane thickness, relative humidity, GDL thickness, N<sub>2</sub> accumulation degree and flow channel depth in descending order. The operating pressure and flow channel depth are negatively correlated with the N<sub>2</sub> crossover coefficient, whereas the others are the opposite.

The parameter importance ranking and the impact rules of the current density regression model are highly consistent with our prior knowledge and previous reports [1,10,13,34,46]. The influence of membrane thickness on cell performance is mainly reflected by the increase in membrane thickness, which leads to an increase in proton transfer resistance and then a decrease in cell performance [47]. The influence of temperature is mainly reflected by the increase in the chemical reaction rate as the elevated temperature accelerates the reaction kinetics. On the other hand, an increase in temperature also leads to an increase in membrane water content and a decrease in membrane proton resistance [48]. An excessive increase in GDL thickness is not preferable to mass transfer inside the cell. An increase in the relative humidity of the feed gas can effectively increase the water content of the proton exchange membrane and reduce the proton transfer resistance. However, it brings some other problems, e.g., water flooding. The increase in flow channel depth can improve cell performance, which is believed to be related to the improved ability of the flow channel to expel liquid water.

For N<sub>2</sub> crossover, the machine learning models also conclude highly consistent with previous reports and prior knowledge [49,50]. Generally, the gas crossover rate is directly proportional to temperature, membrane thickness, relative humidity and GDL thickness but inversely proportional to reactant pressure. The correlations of nitrogen accumulation degree and flow channel depth on the crossover rate are nonmonotonic. This is because the SO<sub>3</sub> at the end of the Nafion molecule of the membrane is strongly hydrophilic. When the membrane is exposed to a humid environment, water binds with SO<sub>3</sub> groups and forms inverted micelles in the polymer matrix, leading to significant expansion of the proton exchange membrane. With the increase in absorbed water, these micelles grow and form interconnected networks,

which promote NGC [15,16]. The main reason for the effect of temperature on gas crossover is that the thermal expansion coefficient of the amorphous phase is larger than that of the crystalline phase. As the temperature rises, the membrane porosity increases due to the difference in the expansion coefficient, which promotes gas crossover.

Although different algorithm models have similar insights, the importance of parameters is slightly different. Therefore, the absolute mean of normalized SHAP values is used to represent the parameter importance. Fig. 8a gathers the parameter importance of all decent algorithms we have inspected in the form of heatmap. However, considering the accuracy of different algorithms, the weight means (WM) of the parameter importance of each algorithm is a more comprehensive evaluation indicator, evaluating results of which are shown in Fig. 8b. The weighting factor equally considering the standardized R<sup>2</sup> and RMSE. The standardization equation is shown in Eq. (57) in SI. The weighted means show that voltage has the greatest influence on current density, with the importance reaching 62%, followed by membrane thickness, temperature, GDL thickness, pressure, nitrogen accumulation degree, relative humidity, and flow channel depth, the parameter importance of which is 20.1%, 8.3%, 3.0%, 2.2%, 1.8%, 1.6% and 0.6%, respectively. Similarly, Figure S7 in the SI shows the parameter importance distribution of the N<sub>2</sub> regression models without E<sub>cell</sub> and T<sub>cc</sub> because the cell voltage is always determined by the actual application and the operating temperature greatly influences the cell performance, which decreases the operational necessity. After weighted treatment, the importance ranking, from significant to insignificant, is air pressure, membrane thickness, relative humidity, GDL thickness, nitrogen accumulation degree and flow channel depth, which are 36%, 33%, 18%, 6.5%, 3.9% and 1.8%, respectively.

It is worth mentioning that the commonly adopted analysis of the global absolute average of SHAP values ignores the local details [51], so it is necessary to further discuss the local rationality of the model. Each parameter is divided into a high parameter range and a low parameter range through the intermediate value. The parameter importance rankings in the high- and low-parameter regions of the XGBoost-based Current density regression model are shown in Fig. 9 and Figure S8 in the SI, for the excellent accuracy and interpretability. We can easily reach the rationality of the variation in the different local regions of all parameters. Here, we illustrate the analysis of N<sub>2</sub> accumulation degree, flow channel depth, membrane thickness and cell voltage.

Instead of simply global analysis with SHAP, segmentation analysis could obtain more detailed information. As shown in Fig. 9a, in the higher nitrogen accumulation region, the importance of membrane thickness and air pressure on cell performance increases, while the importance of temperature and GDL thickness decreases. As nitrogen accumulates at the anode, the overall performance of the cell decreases as the hydrogen supply decreases, resulting in a decline in the production of liquid and absorbed water. Therefore, there is less demand for the water management capability of the cell. Moreover, the cell performance is more sensitive to the change in membrane thickness because the decline in absorbed water content increases the membrane resistance. In the region of lower flow depth, as shown in Fig. 9b, the increase in fluid turbulence promotes the mass transfer efficiency. The parameter importance of nitrogen accumulation, therefore, decreases. The decrease in membrane water content increases the importance of membrane thickness and decreases the importance of operating temperature. Fig. 9c shows that in the region of higher thicker membrane, the influence of membrane thickness on current density is more important than that of the cell voltage. This is because the effect of membrane thickness on membrane resistance is nonlinear. The membrane resistance increases more significantly when the membrane is thicker. This is consistent with the conclusion that the mass transfer efficiency of the membrane is low when the absorbed water in the membrane is low, and the content of bound water in the inner membrane area decreases sharply, leading to a sharp increase in membrane resistance. In Fig. 9d, the importance of temperature, GDL thickness and

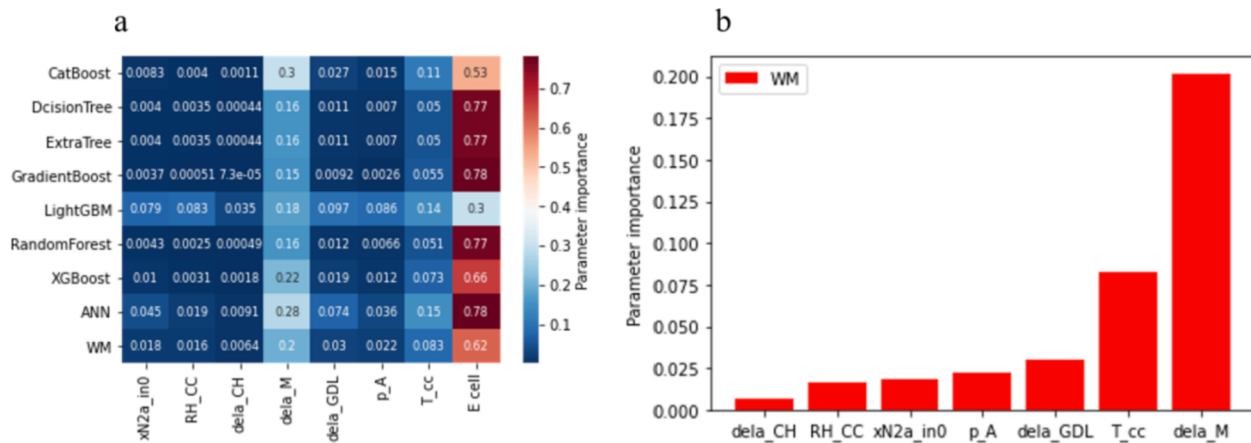


**Fig. 8.** a). Summary of the parameter importance of each algorithm for current density regression on heatmap, b). Parameter importance weight means of all focused decent algorithms.

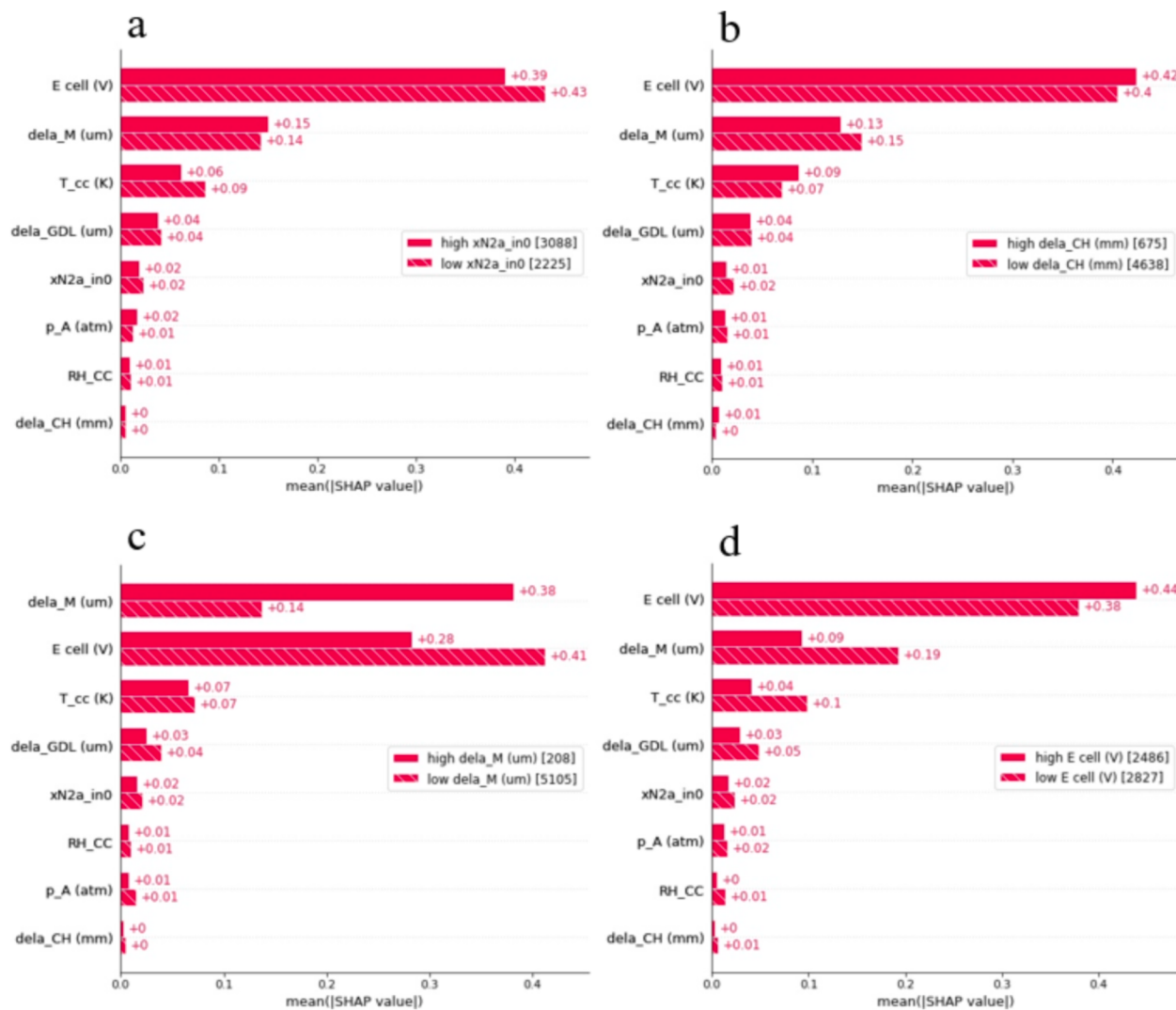


**Fig. 9.** Local parameter importance ranking of XGBoost for current density regression in the dimension of a) N<sub>2</sub> accumulation degree. b) channel depth. c) membrane thickness. d) cell voltage.

nitrogen accumulation in the low voltage region is obviously higher than that in the higher voltage region. It is believed that in the lower voltage region (mass transfer control region), the influence of temperature, GDL

thickness and nitrogen accumulation degree on the internal mass transfer of the cell increases.

### 3.5. $N_2$ Crossover visualization

It is necessary to roughly visualize the distribution of the NGC coefficient, especially for irregular local extrema. The NGC and current density distributions, simulated from ANN (concerning the continuity and accuracy) at the cell voltage 0.7 V are displayed in Fig. 10 and Fig. 11. The distributions at other cell voltages are shown in Figure S9 and Figure S10 in the SI. Through tortuous or even closed-loop contour lines, we can see that the effect of each parameter on NGC does not monotonically increase or decrease. For example, when the  $N_2$  accumulation degree is 0,  $RH_{cc} = 100\%$ ,  $\delta_M = 25 \mu\text{m}$ ,  $P_A = 1 \text{ atm}$ ,  $T_{cc} = 348.15 \text{ K}$ ,  $E_{cell} = 0.7 \text{ V}$ , as shown in Fig. 10b, the distribution of  $N_2$  crossover in two dimensions of flow channel depth and GDL thickness has an obvious peak region and trough region. In addition, when  $RH_{cc} = 100\%$ ,  $\delta_{CH} = 0.5 \text{ mm}$ ,  $\delta_{GDL} = 160 \mu\text{m}$ ,  $P_A = 1 \text{ atm}$ ,  $T_{cc} = 348.15 \text{ K}$ ,  $E_{cell} = 0.7 \text{ V}$ , as shown in Fig. 10d, the optimal value of the membrane thickness also changes under different degrees of nitrogen accumulation. The non-smooth surface is mainly owing to the non-monotonicity of the crossover coefficient both in the dimension of membrane thickness and accumulation degree, the former is majorly caused by the balance of pressure gradient (directly affected by the membrane thickness and boundary conditions) and porosity (directly affected by the transport of solid water in the Nafion molecule of the membrane by micellar network mechanism), the latter is mainly caused by the fuel supply and the corresponding mass transfer, electro-chemical reaction, and heat balance. The coupling of these factors determines the non-smooth distribution surface. Especially

for the studied cases of high  $N_2$  accumulation degree and thin membrane thickness, where the mass transfer of fuels and the balance of the three states of water (vapor, liquid water and dissolved water) are more locally uneven. Similar phenomenon occurs in the distributions of current density as shown in Fig. 11. Therefore, in a 6-dimensional space, it is difficult to seek the global optimum while considering both the performance and NGC. Introducing advanced population optimization algorithms for quicker global optimization is necessary.

### 3.6. Multivariable optimization

Different from traditional global coverage scanning, advanced population optimization algorithms such as the genetic algorithm (GA), particle swarm optimization (PSO) and differential evolution (DE) were adopted in this work. After population initialization, the population constantly changes the search directions through their own experience and the experience of others. Adaptive research rules are always inspired by bionics or other fields. Finally, the optimal fitness and corresponding conditions are determined by judging whether the optimization termination requirements are met. This replaces the inefficient exhaustive global scanning of engineers in the face of high-dimension and high-complexity engineering optimization problems, accelerates the optimization progress, and improves the accuracy and reliability of the conclusions. Then, the fitness function of cell performance and gas crossover is established and optimized to adapt to different application scenarios or application requirements.

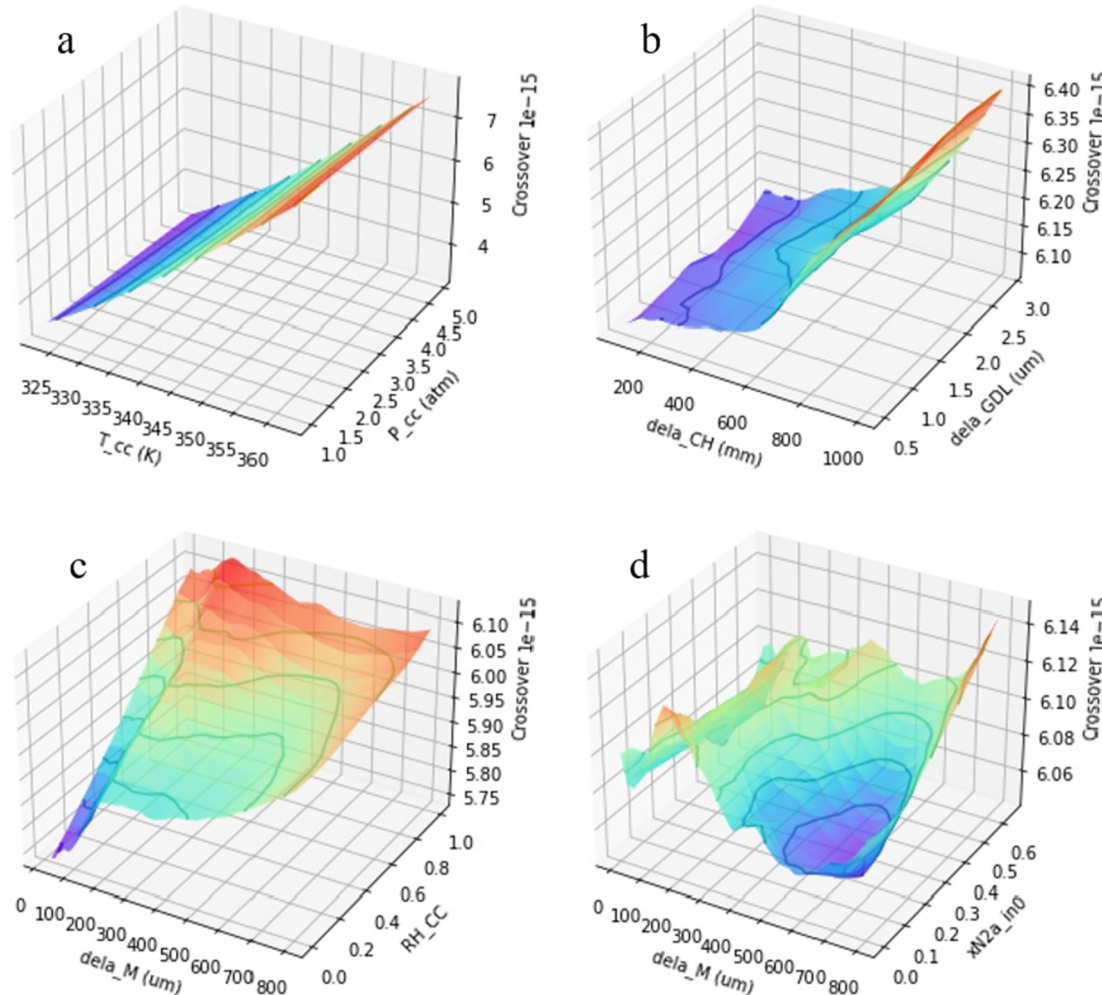


**Fig. 10.** 2D  $N_2$  crossover distribution of a). operating temperature and operating pressure, b). flow channel depth and GDL thickness, c). membrane thickness and relative humidity, and d). membrane thickness and  $N_2$  crossover accumulation degree.

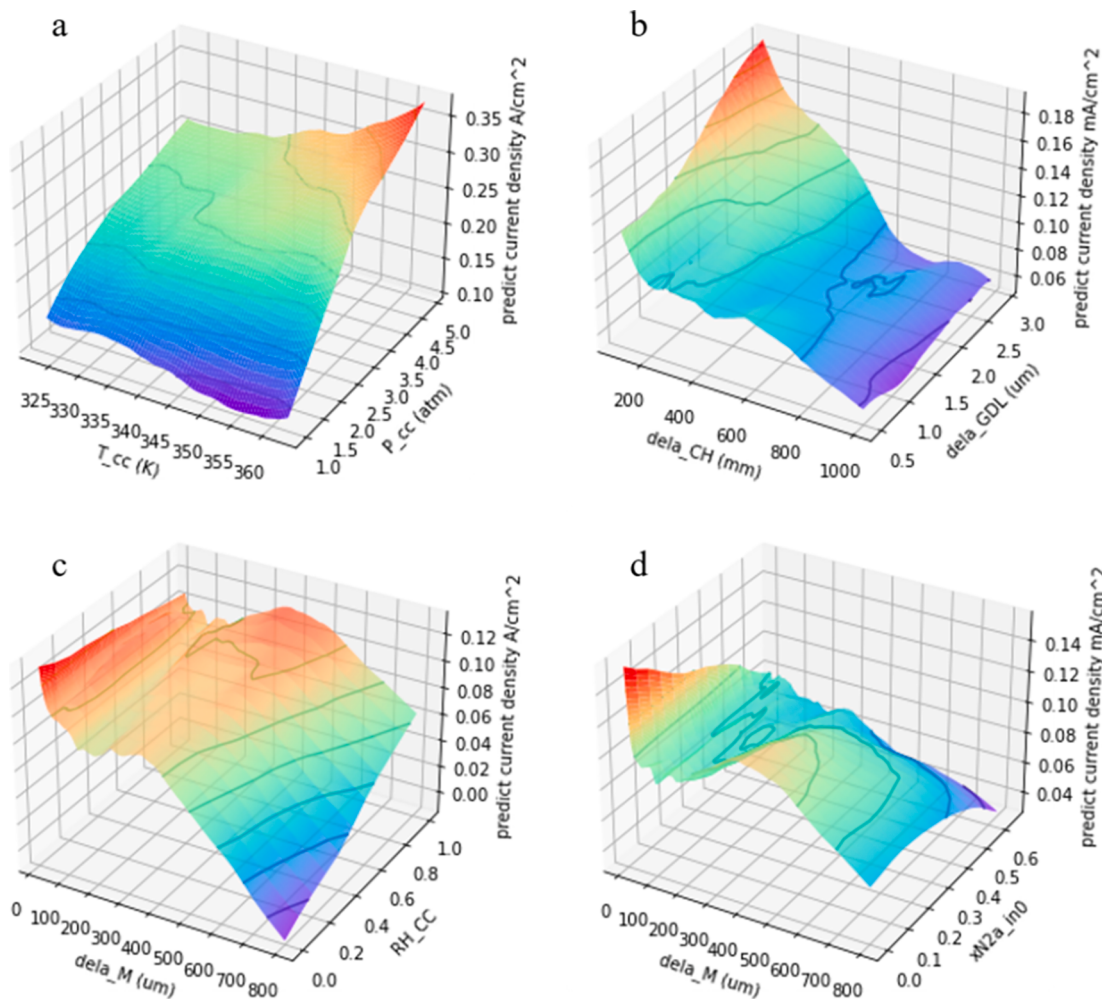


**Fig. 11.** 2D current density distribution of a). operating temperature and operating pressure, b). flow channel depth and GDL thickness, c). membrane thickness and relative humidity, and d). membrane thickness and N<sub>2</sub> crossover accumulation degree.

Take the 6-dimensional optimization of the standardized NGC coefficient, the fitness of this optimization process calculated by Eq. (57) in the SI, as an example to evaluate the optimization algorithms. As shown in Fig. 12, the population optimal fitness lines of a). the genetic algorithm b). the particle swarm optimization algorithm and c). the difference algorithm for the nitrogen crossover coefficient were plotted. On the premise of the same population iteration times, the population iteration times are 156 s, 146 s and 292 s, and the best fitness is -2.05, -2.07 and -2.03, respectively. The particle swarm optimization algorithm, therefore, is the most suitable algorithm for this task.

To evaluate the optimization results, the worst, best and the average

values of current densities and the crossover coefficient were calculated, which quantitatively represents the overall distribution of N<sub>2</sub> crossover and current density, then could be used to build an evaluation system to

**Table 1**  
reference standard.

	Crossover coefficient (mol m <sup>-1</sup> s <sup>-1</sup> Pa <sup>-1</sup> )	Current density (A cm <sup>-2</sup> )
worst	$7.27 \times 10^{-15}$	0.02
average	$4.78 \times 10^{-15}$	1.16
best	$2.30 \times 10^{-15}$	2.30

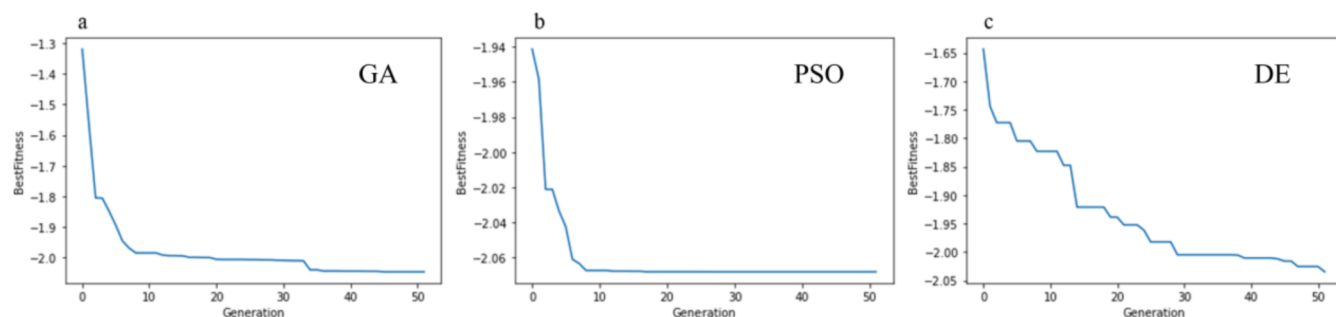


**Fig. 12.** Best fitness plot of NGC coefficient corresponding to a). genetic algorithm (GA), b). particle swarm optimization algorithm (PSO), c). difference algorithm (DE).

fairly appraise and locate the optimization results. The calculated results are shown in Table 1. The corresponding parameter groups are shown in Table S4 in the SI.

Then, the crossover coefficient was optimized in 6 dimensions. The optimization ranges of each parameter could be found in the headline of Table S4 in the SI. The fitness in this optimization process is the standardized crossover coefficient, calculated by Eq. (57) in the SI. Taking the optimization result at 0.7 V when  $N_2$  accumulation is 0 as an example, when  $RH_{cc} = 77\%$ ,  $\delta_{CH} = 0.5 \mu m$ ,  $\delta_M = 10 \mu m$ ,  $\delta_{GDL} = 100 \mu m$ ,  $P_A = 6 \text{ atm}$ , and  $T_{cc} = 323 \text{ K}$ , the best crossover coefficient of  $2.34 \times 10^{-15} \text{ mol m}^{-1} \text{ s}^{-1} \text{ Pa}^{-1}$  is obtained with the corresponding current density of  $1.27 \text{ A cm}^{-2}$ . Compared with the worst condition, the crossover coefficient was decreased by 67.8%, and the current density was improved 66.2 times. In comparison with the average values, the crossover coefficient is decreased by 51.0%, and the current density is improved by 9.7%. Compared with the best condition, The crossover coefficient improved only 1.9%, but the current density decreased 44.7%. Hence, the simple pursuit of a low crossover coefficient might not be practical, and how to maintain a high performance must be considered at the same time.

Since the cell voltage is not stationary in actual operations, it is impossible to reach the best values of both the crossover coefficient and current density. Therefore, we weighted the NGC coefficient and current density in different cell voltages by Eq. (60) and Eq. (61) in the SI. The assumptive weight coefficient is shown in Figure S11 in the SI. To consider both performance indicators, a new fitness when  $N_2$  accumulation is 0,  $F_n(a, b)$ , was built by weighting the weighted crossover coefficient and current density, as shown in Eq. (62) in the SI.

We optimized  $F_n(0.5, 0.5)$ , which means equally considering the crossover coefficient and the current density. When  $RH_{cc} = 100\%$ ,  $\delta_{CH} = 2.32 \mu m$ ,  $\delta_M = 10 \mu m$ ,  $\delta_{GDL} = 100 \mu m$ ,  $P_A = 3.7 \text{ atm}$  and  $T_{cc} = 323 \text{ K}$ , it meets the best fitness value of  $-2.73$ . The best fitness curve and the distribution of the optimization result is shown in Fig. 13, where the blue point is the optimum found by PSO and the red ones are the random sampling points in the 6-dimensions parameter space. Therefore, the location and the density of the red points can reflect the global distribution of the compound-objective. Compared with the average crossover coefficient of  $4.78 \times 10^{-15} \text{ mol m}^{-1} \text{ s}^{-1} \text{ Pa}^{-1}$ , the best crossover coefficient of  $2.41 \times 10^{-15} \text{ mol m}^{-1} \text{ s}^{-1} \text{ Pa}^{-1}$  is decreased by 49.5%. Compared with the average current density of  $1.16 \text{ A cm}^{-2}$ , the best current density is increased by 19%. Therefore, an ideal design parameters that equally considers the crossover coefficient and the current density could be obtained.

As for the reliability of the optimization results, three different optimization algorithms are repeated five times with random initialization. Compared with results from GA and DE that showed large difference, PSO could precisely found the global optimum each time. As shown in Fig. 14, the fluctuation range (difference between the optimum

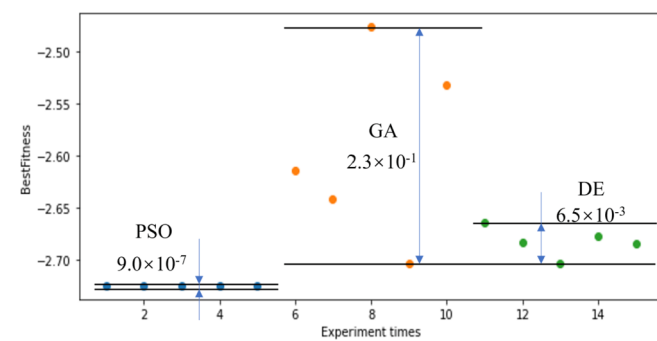


Fig. 14. Five times repeated optimization results of PSO, GA and DE.

found each time) is kept less than  $10^{-6}$  while the variance of them is kept less than  $10^{-12}$ . Therefore, PSO has proven itself not only to be the fastest (as previously mentioned) but also the most robust optimization algorithm. Brief introduction of PSO algorithm is available in the SI.

Further fitness evaluations on both the traditional MNM method and the MNM-ML strategy are accomplished. The distribution pattern of current densities and nitrogen crossover coefficients obtained by skeletally scanning the MNM, namely the dataset used for training machine learning models is shown in Fig. 15, indicated that the mean relative sampling interval of all dimensions of the database was above 10%. By traditional methods, the precision of our optimized results is the same as the mean relative interval and costs more than 22 days. The mean relative error (MRE) of the MNM-ML strategy is lower than 2% according to previous results in Fig. 4. If we want to obtain the same precision of the optimization result with the same fineness by the grid searching on the MNMs, the mean relative sampling interval should be 1/5 of what it used to be. Thereby, the computational time would be 5<sup>6</sup> times longer. Moreover, researchers can study the functional rule of each parameter assisted by ML and build new fitness equations for more practical needs, which are infinitely malleable and more intelligent.

#### 4. Conclusions

In this paper, a new approach, machine learning-assisted multi-physics numerical model (MNM-ML), was proposed and standardized to accelerate the optimization of mitigation strategies for NGC. Firstly, a two-dimensional steady-state mechanistic model was accomplished and experimentally validated to construct a database of six parameters that greatly affect the cell current density and nitrogen gas crossover (NGC). Secondly, nine algorithms widely used in the field of machine learning are trained, optimized through hyperparameter adaptive grid search and explained by SHAP. Then, the best machine learning models for current density and NGC coefficient regression were obtained by algorithm

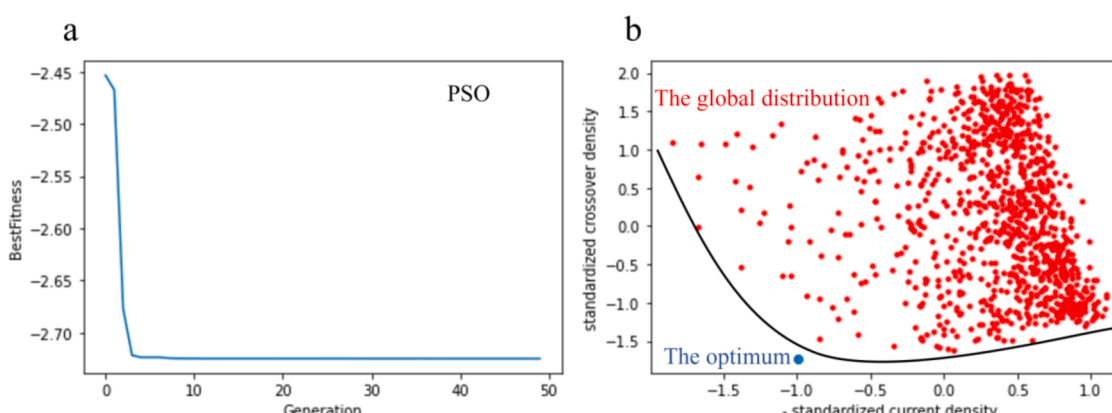
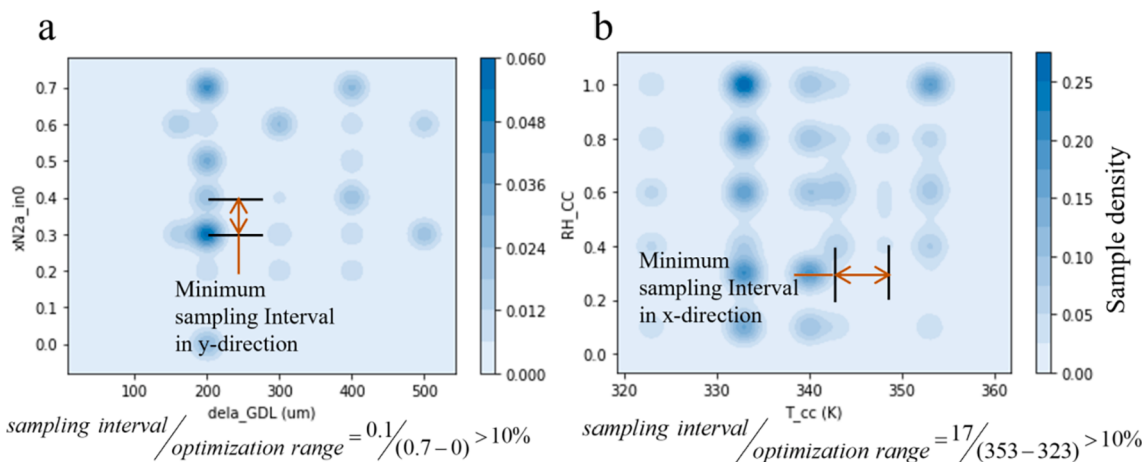


Fig. 13. a). Best fitness curve of the optimization of  $F_n(0.5, 0.5)$  by PSO, b). The distribution of optimization solution.



**Fig. 15.** Data set distribution in 2 dimensions of a)  $N_2$  accumulation and GDL thickness. b) relative humidity and operating temperature. (The color gradient was determined by the sample density).

competition. Finally, population optimization algorithms were used to search for the global optimal combination of the 6 studied parameters. The main findings of this research are summarized as follows:

a).  $N_2$  accumulation greatly decreases the performance of the PEM fuel cells. The maximum cell power density loss is 28.9%, as measured.  
b). The distribution of the NGC coefficient in a 6-dimensional parameter space indicates that the effect of each parameter on NGC is nonmonotonic. Therefore, it is necessary to introduce some advanced strategies for quicker global optimization.

c). Innovatively segmenting the parameter space to seek and validate the local mechanism of each parameter, regression path comparison and parameter importance ranking reinforce the reliability of machine learning models.

d). In our optimization range, the best fitness (a composite optimization goal we built in section 3.6) is achieved when the relative humidity, flow channel depth, membrane thickness, GDL thickness, operating pressure and operating temperature are 100%, 2.32 mm, 10  $\mu\text{m}$ , 100  $\mu\text{m}$ , 3.7 atm and 323 K, respectively.

e). The NGC coefficient is decreased by 49.5%, with the cell performance improves by 20%, after optimization by the developed MNM-ML model. Moreover, the computational time is greatly reduced.

#### Declaration of Competing Interest

The authors declare that they have no known competing financial interests or personal relationships that could have appeared to influence the work reported in this paper.

#### Acknowledgements

This work was supported by the Joint Fund of Ministry of Education for Equipment Pre-research [6141A02022531] and National Natural Science Foundation of China [21978118].

#### Appendix A. Supplementary data

Supplementary data to this article can be found online at <https://doi.org/10.1016/j.cej.2022.136064>.

#### References

- [1] K. Promislow, J. St-Pierre, B. Wetton, A simple, analytic model of polymer electrolyte membrane fuel cell anode recirculation at operating power including nitrogen crossover, *J. Power Sources* 196 (23) (2011) 10050–10056, <https://doi.org/10.1016/j.jpowsour.2011.08.070>.
- [2] S. Abbou, J. Dillet, G. Maranzana, S. Didierjean, O. Lottin, Local potential evolutions during proton exchange membrane fuel cell operation with dead-ended anode – Part II: Aging mitigation strategies based on water management and nitrogen crossover, *J. Power Sources* 340 (2017) 419–427, <https://doi.org/10.1016/j.jpowsour.2016.10.045>.
- [3] H. Karimäki, L.C. Pérez, K. Nikiforow, T.M. Keränen, J. Viitakangas, J. Ihonen, The use of on-line hydrogen sensor for studying inert gas effects and nitrogen crossover in PEMFC system, *Int. J. Hydrogen Energy* 36 (16) (2011) 10179–10187, <https://doi.org/10.1016/j.ijhydene.2011.04.230>.
- [4] D. Bessarabov, P. Kozak, Measurement of gas permeability in SPE membranes for use in fuel cells, *Membr. Technol.* 2007 (12) (2007) 6–9, [https://doi.org/10.1016/s0958-2118\(07\)70264-1](https://doi.org/10.1016/s0958-2118(07)70264-1).
- [5] A.Z. Weber, Gas-crossover and membrane-pinhole effects in polymer-electrolyte fuel cells, *J. Electrochem. Soc.* 155 (6) (2008), <https://doi.org/10.1149/1.2898130>.
- [6] E. Alizadeh, M. Rahimi-Esbo, S.M. Rahgoshay, S.H.M. Saadat, M. Khorshidian, Numerical and experimental investigation of cascade type serpentine flow field of reactant gases for improving performance of PEM fuel cell, *Int. J. Hydrogen Energy* 42 (21) (2017) 14708–14724, <https://doi.org/10.1016/j.ijhydene.2017.04.212>.
- [7] A. Rabbani, M. Rokni, Effect of nitrogen crossover on purging strategy in PEM fuel cell systems, *Appl. Energy* 111 (2013) 1061–1070, <https://doi.org/10.1016/j.apenergy.2013.06.057>.
- [8] T.-T. Nguyen, K. Fushinobu, Effect of operating conditions and geometric structure on the gas crossover in PEM fuel cell, *Sustainable Energy Technol. Assess.* 37 (2020), <https://doi.org/10.1016/j.seta.2019.100584>.
- [9] K.D. Baik, M.S. Kim, Characterization of nitrogen gas crossover through the membrane in proton-exchange membrane fuel cells, *Int J Hydrogen Energ* 36 (1) (2011) 732–739, <https://doi.org/10.1016/j.ijhydene.2010.09.046>.
- [10] J. Nam, P. Chippa, W. Kim, H. Ju, Numerical analysis of gas crossover effects in polymer electrolyte fuel cells (PEFCs), *Appl. Energy* 87 (12) (2010) 3699–3709, <https://doi.org/10.1016/j.apenergy.2010.05.023>.
- [11] P. Chippa, H. Ju, Numerical modeling and investigation of gas crossover effects in high temperature proton exchange membrane (PEM) fuel cells, *Int. J. Hydrogen Energy* 38 (18) (2013) 7704–7714, <https://doi.org/10.1016/j.ijhydene.2012.07.123>.
- [12] A. Jung, M.S. Kim, *Gas Crossover in Polymer Electrolyte Membranes*, ECS Trans. 69 (2015) 561–568.
- [13] K.D. Baik, B.K. Hong, M.S. Kim, Effects of operating parameters on hydrogen crossover rate through Nafion® membranes in polymer electrolyte membrane fuel cells, *Renewable Energy* 57 (2013) 234–239, <https://doi.org/10.1016/j.renene.2013.01.046>.
- [14] S.S. Kocha, J. Deliang Yang, J.S. Yi, Characterization of gas crossover and its implications in PEM fuel cells, *AIChE Journal* 52(5) (2006) 1916–1925, <https://doi.org/10.1002/aijc.10780>.
- [15] L. Zhang, C. Ma, S. Mukerjee, Oxygen permeation studies on alternative proton exchange membranes designed for elevated temperature operation, *Electrochim. Acta* 48 (13) (2003) 1845–1859, [https://doi.org/10.1016/s0013-4686\(03\)00257-3](https://doi.org/10.1016/s0013-4686(03)00257-3).
- [16] S. Kreitmeier, P. Lerch, A. Wokaun, F.N. Büchi, Local degradation at membrane defects in polymer electrolyte fuel cells, *J. Electrochem. Soc.* 160 (4) (2013) F456–F463, <https://doi.org/10.1149/1.023306jcs>.
- [17] W. Li, Q. Zhang, C. Wang, X. Yan, S. Shen, G. Xia, F. Zhu, J. Zhang, Experimental and numerical analysis of a three-dimensional flow field for PEMFCs, *Appl. Energy* 195 (2017) 278–288, <https://doi.org/10.1016/j.apenergy.2017.03.008>.
- [18] N.T. Truc, S. Ito, K. Fushinobu, Numerical and experimental investigation on the reactant gas crossover in a PEM fuel cell, *Int. J. Heat Mass Transf.* 127 (2018) 447–456, <https://doi.org/10.1016/j.ijheatmasstransfer.2018.07.092>.
- [19] R. Ding, Y.W. Chen, P. Chen, R. Wang, J.K. Wang, Y.Q. Ding, W.J. Yin, Y.D. Liu, J. Li, J.G. Liu, Machine learning-guided discovery of underlying decisive factors and new mechanisms for the design of nonprecious metal electrocatalysts, *Accts Catal* 11 (15) (2021) 9798–9808, <https://doi.org/10.1021/acscatal.1c01473>.

- [20] R. Ding, R. Wang, Y.Q. Ding, W.J. Yin, Y.D. Liu, J. Li, J.G. Liu, Designing AI-Aided analysis and prediction models for nonprecious metal electrocatalyst-based proton-exchange membrane fuel cells, *Angew Chem Int Ed* 59 (43) (2020) 19175–19183, <https://doi.org/10.1002/anie.202006928>.
- [21] Z.G. Hua, Z.X. Zheng, E. Pahon, M.C. Pera, F. Gao, Remaining useful life prediction of PEMFC systems under dynamic operating conditions, *Energ Convers Manage* 231 (2021) 113825, <https://doi.org/10.1016/j.enconman.2021.113825>.
- [22] L. Xing, X.G. Song, K. Scott, V. Pickert, W.P. Cao, Multi-variable optimisation of PEMFC cathodes based on surrogate modelling, *Int J Hydrogen Energ* 38 (33) (2013) 14295–14313, <https://doi.org/10.1016/j.ijhydene.2013.08.104>.
- [23] N. Khajeh-Hosseini-Dalasm, M. Fesanghary, K. Fushinobu, K. Okazaki, A study of the agglomerate catalyst layer for the cathode side of a proton exchange membrane fuel cell: Modeling and optimization, *Electrochim. Acta* 60 (2012) 55–65, <https://doi.org/10.1016/j.electacta.2011.10.099>.
- [24] Y. Li, Z. Zhou, X. Liu, W.-T. Wu, Modeling of PEM fuel cell with thin MEA under low humidity operating condition, *Appl. Energy* 242 (2019) 1513–1527, <https://doi.org/10.1016/j.apenergy.2019.03.189>.
- [25] L. Xing, M. Mamlouk, R. Kumar, K. Scott, Numerical investigation of the optimal Nafion® ionomer content in cathode catalyst layer: An agglomerate two-phase flow modelling, *Int. J. Hydrogen Energy* 39 (17) (2014) 9087–9104, <https://doi.org/10.1016/j.ijhydene.2014.03.225>.
- [26] L. Xing, Q. Cai, C. Xu, C. Liu, K. Scott, Y. Yan, Numerical study of the effect of relative humidity and stoichiometric flow ratio on PEM (proton exchange membrane) fuel cell performance with various channel lengths: An anode partial flooding modelling, *Energy* 106 (2016) 631–645, <https://doi.org/10.1016/j.energy.2016.03.105>.
- [27] L. Xing, X. Liu, T. Alaje, R. Kumar, M. Mamlouk, K. Scott, A two-phase flow and non-isothermal agglomerate model for a proton exchange membrane (PEM) fuel cell, *Energy* 73 (2014) 618–634, <https://doi.org/10.1016/j.energy.2014.06.065>.
- [28] L. Xing, An agglomerate model for PEM fuel cells operated with non-precious carbon-based ORR catalysts, *Chem. Eng. Sci.* 179 (2018) 198–213, <https://doi.org/10.1016/j.ces.2018.01.026>.
- [29] L. Xing, Y. Wang, P.K. Das, K. Scott, W. Shi, Homogenization of current density of PEM fuel cells by in-plane graded distributions of platinum loading and GDL porosity, *Chem. Eng. Sci.* 192 (2018) 699–713, <https://doi.org/10.1016/j.ces.2018.08.029>.
- [30] L. Xing, Q. Cai, X. Liu, C. Liu, K. Scott, Y. Yan, Anode partial flooding modelling of proton exchange membrane fuel cells: Optimisation of electrode properties and channel geometries, *Chem. Eng. Sci.* 146 (2016) 88–103, <https://doi.org/10.1016/j.ces.2016.02.029>.
- [31] B. Wang, K. Wu, F. Xi, J. Xuan, X. Xie, X. Wang, K. Jiao, Numerical analysis of operating conditions effects on PEMFC with anode recirculation, *Energy* 173 (2019) 844–856, <https://doi.org/10.1016/j.energy.2019.02.115>.
- [32] L. Xing, Y. Xu, Z. Penga, Q. Xu, H. Su, W. Shi, F. Barbir, A novel flow field with controllable pressure gradient to enhance mass transport and water removal of PEM fuel cells, *AIChE J.* 66 (6) (2020), <https://doi.org/10.1002/aic.16957>.
- [33] M. Inaba, T. Kinumoto, M. Kiriakie, R. Umebayashi, A. Tasaka, Z. Ogumi, Gas crossover and membrane degradation in polymer electrolyte fuel cells, *Electrochim. Acta* 51 (26) (2006) 5746–5753, <https://doi.org/10.1016/j.electacta.2006.03.008>.
- [34] B. Bensmann, R. Hanke-Rauschenbach, K. Sundmacher, In-situ measurement of hydrogen crossover in polymer electrolyte membrane water electrolysis, *Int. J. Hydrogen Energy* 39 (1) (2014) 49–53, <https://doi.org/10.1016/j.ijhydene.2013.10.085>.
- [35] T.Q. Chen, C. Guestrin, XGBoost: A Scalable Tree Boosting System, *Kdd'16*, in: *Proceedings of the 22nd ACM SIGKDD International Conference on Knowledge Discovery and Data Mining*, 2016, pp. 785–794, <https://doi.org/10.1145/2939672.2939785>.
- [36] R.S. Hu, X.L. Li, Y.X. Zhao, Gradient boosting learning of hidden Markov models, *Int Conf Acoust Spee* (2006) 1165–1168.
- [37] L. Prokhorenko, G. Gusev, A. Vorobev, A.V. Dorogush, A. Gulin, CatBoost: unbiased boosting with categorical features, *Adv Neur In* 31 (2018).
- [38] L. Breiman Random forests *Mach Learn* 45 1 10.1023/A:1010933404324. 2001, pp. 5–32 <https://doi.org/Doi>.
- [39] P. Geurts, D. Ernst, L. Wehenkel, Extremely randomized trees, *Mach Learn* 63 (1) (2006) 3–42, <https://doi.org/10.1007/s10994-006-6226-1>.
- [40] M. Dumont, R. Maree, L. Wehenkel, P. Geurts, Fast Multi-Class Image Annotation with Random Subwindows and Multiple Output Randomized Trees, in: *Visapp 2009: Proceedings of the Fourth International Conference on Computer Vision Theory and Applications*, Vol 2, 2009, p. 196–+.
- [41] G.L. Ke, Q. Meng, T. Finley, T.F. Wang, W. Chen, W.D. Ma, Q.W. Ye, T.Y. Liu, LightGBM: A Highly Efficient Gradient Boosting Decision Tree, *Advances in Neural Information Processing Systems* 30 (Nips 2017) 30 (2017).
- [42] B. Kégl, The return of AdaBoost. MH: multi-class Hamming trees, *arXiv preprint arXiv:1312.6086* (2013).
- [43] J. Schmidhuber, Deep learning in neural networks: An overview, *Neural networks* 61 (2015) 85–117.
- [44] M.T. Ribeiro, S. Singh, C. Guestrin, Why Should I Trust You?, in: *Proceedings of the 22nd ACM SIGKDD International Conference on Knowledge Discovery and Data Mining*, 2016, pp. 1135–1144.
- [45] A. Shrikumar, P. Greenside, A. Kundaje, Learning Important Features Through Propagating Activation Differences, in: P. Doina, T. Yee Whye (Eds.) *Proceedings of the 34th International Conference on Machine Learning*, PMLR, *Proceedings of Machine Learning Research*, 2017, pp. 3145–3153.
- [46] X. Cheng, J. Zhang, Y. Tang, C. Song, J. Shen, D. Song, J. Zhang, Hydrogen crossover in high-temperature PEM fuel cells, *J. Power Sources* 167 (1) (2007) 25–31, <https://doi.org/10.1016/j.jpowsour.2007.02.027>.
- [47] S. Mohanty, A.N. Desai, S. Singh, V. Ramadesigan, S. M, Effects of the membrane thickness and ionomer volume fraction on the performance of PEMFC with U-shaped serpentine channel, *International Journal of Hydrogen Energy* 46(39) (2021) 20650–20663. <https://doi.org/https://doi.org/10.1016/j.ijhydene.2021.03.252>.
- [48] C.-Y. Jung, H.-S. Shim, S.-M. Koo, S.-H. Lee, S.-C. Yi, Investigations of the temperature distribution in proton exchange membrane fuel cells, *Appl. Energy* 93 (2012) 733–741, <https://doi.org/10.1016/j.apenergy.2011.08.035>.
- [49] O.S. Ijaodola, Z. El Hassan, E. Ogungbemi, F.N. Khatib, T. Wilberforce, J. Thompson, A.G. Olabi, Energy efficiency improvements by investigating the water flooding management on proton exchange membrane fuel cell (PEMFC), *Energy* 179 (2019) 246–267, <https://doi.org/10.1016/j.energy.2019.04.074>.
- [50] C. Tsinos, L. Apekidis, P. Pissis, Water sorption and dielectric relaxation spectroscopy studies in hydrated Nafion® (-SO<sub>3</sub>K) membranes, *J. Mater. Sci.* 35 (23) (2000) 5957–5965, <https://doi.org/10.1023/A:1026782509106>.
- [51] R. Ding, W. Yin, G. Cheng, Y. Chen, J. Wang, R. Wang, Z. Rui, J. Li, J. Liu, Boosting the optimization of membrane electrode assembly in proton exchange membrane fuel cells guided by explainable artificial intelligence, *Energy and AI* 5 (2021), 100098, <https://doi.org/10.1016/j.egyai.2021.100098>.